Efficient Aperture Illumination and Beamforming with Huygens' Metasurfaces Exciting Surface Waves

Vasileios G. Ataloglou*, George V. Eleftheriades
The Edward S. Rogers Sr. Department of Electrical and Computer Engineering University of Toronto, Toronto, Canada
*vasilis.ataloglou@mail.utoronto.ca

***Abstract*—Huygens' metasurfaces allow for extreme wave manipulation of the incident fields. Their ability to shape the electromagnetic wavefronts have made them a promising platform to build antenna systems without complicated feeding networks. However, for conventional passive and lossless Huygens' metasurfaces, the power density of the incident and output fields should be locally conserved. This requirement poses limitations to the amplitude of the output fields, especially if the radiating source is placed close to the metasurface. In this paper, a method is proposed to bypass these limitations and design Huygens' metasurfaces with nonlocal response. The method relies on surface waves that redistribute the power in the input side of the metasurface. The usefulness is demonstrated through the design of a radiating aperture with directivity beyond that of conventional metasurfaces. Furthermore, a physical Huygens' metasurface is designed to realize a singly-fed Taylor aperture antenna, verifying the potential of accurate and efficient beamforming.**

***Index Terms*—Huygens' metasurfaces, surface waves, aperture efficiency, beamforming**

I. Introduction

Antenna engineering requires control over various radiation characteristics of the antenna, such as the directivity, the beamwidth and the sidelobe level. To satisfy these requirements, traditional antenna systems have been realized with antenna arrays using well-established design methods [1]. In principle, the amplitude and phase of the currents at each element are independently controlled in order to realize the desired far-field radiation pattern. However, the requirement of sophisticated feeding networks increases significantly the total size and power losses of antenna arrays, potentially rendering them impractical for the growing demand of compact and low-power antennas in today's applications (e.g. Internet of Things, 5G communications, automotive radars).

Metasurfaces provide a useful platform to address the aforementioned issues of antenna arrays. Specifically, Huygens' metasurfaces (HMSs) consist of orthogonally polarized electric and magnetic dipole moments that are arranged in a thin sheet [2], [3]. Acting as secondary sources, that are passively excited from the incident fields, these dipole moments offer great capabilities at shaping the electromagnetic wavefronts and realizing directive beams at the far-field region. Metasurfaces can be illuminated by a single source and are usually realized with a few subwavelength copper layers; therefore, they are low-profile and they do not require complex feeding networks. However, to realize highly-directive radiated beams, an effective illumination of the aperture is necessary. In particular, passive and lossless Huygens' metasurface have to satisfy local power conservation, even in the case that omega-bianisotropy is present [4]. Therefore, the output fields of an HMS have to adhere to the incident power profile, limiting the directivity that can be obtained for a specific aperture length and source illumination. The constraints become more evident when the source is placed close to the HMS, such as in conventional metasurface lenses with a small f/D (focal length/diameter) ratio [5].

Different methods have been studied and demonstrated to alleviate the local power conservation limitations of HMSs, including a cavity-excited metasurface and HMS pairs [6]–[8]. However, the use of a metallic cavity and the required separation distance, respectively, still lead to fairly bulky designs. On the other hand, surface waves have demonstrated nonlocal interactions and they have been utilized for beam splitting, cloaking and beam forming in the reflection mode [9]–[11]. In this work, we harness the capability of surface waves to effectively redistribute the incident power in order to design an HMS with nearly-unity aperture illumination efficiency, as well as to show antenna beamforming in the transmission mode. The required surface distribution is determined upon a power-based point matching technique at the HMS boundary and optimization to minimize the average power mismatch. Then, the effective parameters of the omega-bianisotropic HMS can be calculated using analytical expressions that involve the tangential fields at the two sides [4].

The rest of the paper is organized as follows. Section II describes briefly the design method to determine the surface waves for a particular transformation. The method is employed in Sec. III to demonstrate high aperture efficiency for broadside and tilted radiated beams. A physical realization with a 4-layer structure is presented for a Taylor pattern singly-fed antenna in Sec. IV, while conclusions are made in Sec. V.

II. Method for determining surface-waves

The problem under consideration is sketched in Fig. 1. The incident fields $\{\mathbf{E}_{\text{inc}}, \mathbf{H}_{\text{inc}}\}$, emanated from a single source S, illuminate a passive and lossless HMS of length L_{tot} located at the plane $y = 0$. The output fields $\{\mathbf{E}_{\text{out}}, \mathbf{H}_{\text{out}}\}$ have

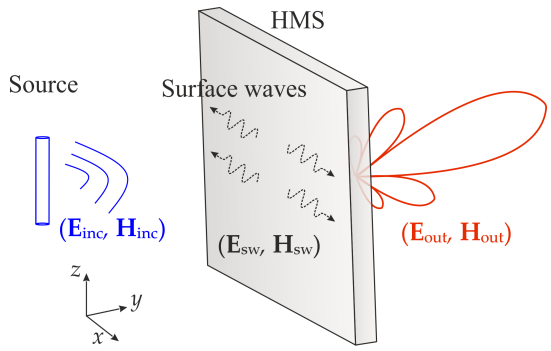

Fig. 1. Schematic of surface-wave assisted beamforming with a single HMS.

prescribed amplitude and phase profiles based on the desired radiation characteristics of the aperture, while at the same time all of the incident power needs to be transmitted to the output. Normally, the different power profiles at the two sides of the HMS would incur reflections or require regions exhibiting loss and gain. However, by means of auxiliary surface waves $\{\mathbf{E}_{\rm sw}, \mathbf{H}_{\rm sw}\}$, that are passively excited from the HMS, it is possible to restore the local power conservation condition and design a passive omega-bianisotropic HMS harnessing all the incident power. For simplicity, in what follows we consider uniformity along the z-axis and transverse-magnetic (TM) polarized fields ($\mathbf{H} = H^z\hat{\mathbf{z}}$).

In order to calculate the necessary surface waves, we expand the magnetic field H^z_{sw} at the plane $y = 0^-$ to the following set of basis functions,

$$H^z_{\rm sw}(x) = \sum_{n=-N}^{n=N} A_n \frac{\sin(k_w(x-nL))}{k_w(x-nL)} \cos(k_c(x-nL)), \quad (1)$$

where A_n are unknown complex weights to be determined, k_w and k_c are two parameters that control the spectrum of the surface waves, $2N+1$ is the total number of sampling points (unit cells) and $L = L_{\rm tot}/(2N+1)$ is the distance between them. This class of sinc-type basis functions has been selected for a similar method of designing metasurface pairs [12], as it avoids any discretization in terms of wavenumbers k_x and allows control of the range of added spectrum. However, in this work the sinc functions are modulated at a frequency k_c so that their spectrum is purely evanescent. Specifically, by taking the Fourier transform of (1), the spectrum is found to be non-zero only for $k_c - k_w \leq |k_x| \leq k_c + k_w$. By choosing $k_c - k_w \geq k$ (k standing for the free-space wavenumber), it is ensured that the spectrum is purely evanescent and the far-field region of the metasurface is not perturbed.

The corresponding tangential electric field $E^x_{\rm sw}$ is also expressed at $y = 0^-$ as a function of the weights A_n through a plane wave decomposition of the magnetic field defined in (1). Then, the total input fields $\{E^x_{\rm in}, H^z_{\rm in}\}$ are calculated by summing up the contributions of the incident fields and the auxiliary surface waves. This allows to calculate the normal power density at the input of the metasurface $P_{\rm in}(x)$ in the presence of the surface waves as a function of the weights A_n. In order for the power to be locally conserved, the input power density profile $P_{\rm in}(x)$ should match the output power density profile $P_{\rm out}(x)$. This condition is applied to the center of the $2N+1$ unit cells across the metasurface forming a nonlinear system of equations for the unknown weights A_n as below,

$$\mathbf{G} = \left(P_{\rm in}(y=0^-) - P_{\rm out}(y=0^+)\right)\Big|_{x=nL} = 0, \quad (2)$$

where the rows of vector $\mathbf{G}$ represent the different matching points across the HMS.

Since the above system of equations cannot be tackled analytically, a gradient descent optimization method is employed to minimize the average power mismatch at the selected sampling points by minimizing $F = \mathbf{G}^T\mathbf{G}/2$. As a result of this process, the weights A_n are determined and the necessary surface waves to redistribute the power are fully defined through (1). It is noted that for most practical scenarios, including the ones presented in the rest of the paper, some basic tuning of the optimization parameters (starting point, learning rate, etc.) was sufficient to get solutions with very low (less than 5%) power mismatch for all unit cells. Once the optimization is converged and given that the power mismatch is sufficiently low, an omega-bianisotropic HMS can be designed as passive and lossless. Specifically, the electric surface impedance $Z_{\rm se}(x)$, the magnetic surface admittance $Y_{\rm sm}(x)$ and the magnetoelectric coupling coefficient $K_{\rm em}(x)$ of the HMS are specified at each sampling point, based on the total tangential fields at the two sides. Finally, these parameters can be realized with three lossless impedance sheets to verify the model or with physical unit cells to study practical aspects, as it will be described in the following sections.

III. Efficient Illumination of Large Apertures

Auxiliary surface waves can be advantageous in cases that highly-directive beams are required at the output of a large radiating aperture/metasurface and the source is placed close to the HMS to minimize the total size. In the following we consider an infinite (along z) magnetic current line-source that is placed $s = \lambda/3$ away from an HMS of length $L_{\rm tot} = 8\lambda$. The wavelength $\lambda \approx 30$ mm corresponds to the operating frequency of 10 GHz. The purpose is to utilize the framework outlined in Sec. II to obtain maximum directivity at broadside at the output.

The incident fields from the source at $(x, y) = (0, -\lambda/3)$ are analytically calculated at $y = 0^-$ as

$$H^z_{\rm inc}(x) = -\frac{k}{4\eta} H^{(2)}_0\left(k\sqrt{x^2 + (\lambda/3)^2}\right), \quad (3)$$

$$E^x_{\rm inc}(x) = -\frac{jk}{4} \frac{\lambda/3}{\sqrt{x^2 + (\lambda/3)^2}} H^{(2)}_1\left(k\sqrt{x^2 + (\lambda/3)^2}\right), \quad (4)$$

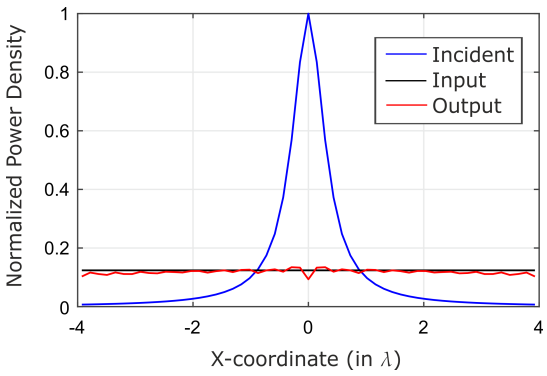

Fig. 2. Incident, input and output power densities for a required uniform output aperture. The introduction of surface waves restores local power conservation allowing a passive and lossless HMS to perform the wave transformation.

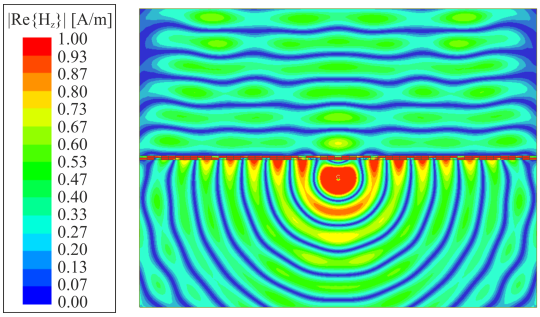

Fig. 3. Magnetic field $|\mathrm{Re}\{H_z\}|$ from full-wave simulations. The incident power from a source $\lambda/3$ before the HMS is redistributed along the boundary via the auxiliary surface wave distribution to form a uniform planar output.

where $H_n^{(2)}$ is the n-th order Hankel function of second kind. Aiming at maximum directivity, a uniform output profile extending from $-L_{\mathrm{tot}}/2$ to $L_{\mathrm{tot}}/2$ is selected, specifically

$$H^z_{\mathrm{out}}(x) = \frac{A}{\sqrt{\cos(\theta_{\mathrm{out}})}}\exp\{-jk\sin(\theta_{\mathrm{out}})x\}, \quad (5)$$

$$E^x_{\mathrm{out}}(x) = A\sqrt{\cos(\theta_{\mathrm{out}})}\exp\{-jk\sin(\theta_{\mathrm{out}})x\}, \quad (6)$$

where θ_{out} is the angle of the desired output beam and A is a normalization constant so that the total output power becomes equal to the total incident power. Of course, for broadside radiation, it should be $\theta_{\mathrm{out}} = 0$. The incident and output power profiles are considerably different, as it can be observed from Fig. 2. Surface waves are then utilized to restore the local power conservation without incurring reflected propagating power. In particular, the wavenumber parameters are set to $k_w = 1.1k$ and $k_c = 2.1k$, while the sampling points are $2N+1 = 55$. The converged solution shows a great matching of the total input and output power densities, as seen in Fig. 2.

Each unit cell is modeled with three lossless impedance sheets, separated by dielectric substrates of dielectric constant $\epsilon_r = 11.2$ and thickness $t = 1.27$ mm. Based on a transmission-line model the values of the impedances can be analytically calculated to implement the required HMS parameters of each unit cell [4]. Furthermore, perfect electric (PEC) walls are used as buffers to reduce intercell coupling and restore rectilinear propagation as proposed in [13]. The HMS is simulated with the commercial software Ansys HFSS with the source modeled as a small current loop in periodic boundary conditions (along z). The real part of the magnetic field is depicted in Fig 3. It is clear that the cylindrical wave from the source takes the form of a plane wave at the output with approximately constant amplitude as desired. Higher field values due to the induced surface waves can be also observed at the input side of the HMS. However, these waves are confined in the vicinity of the HMS and do not result in real reflected power.

Different metrics can be calculated to assess the efficiency of the proposed HMS. First of all, power transmission efficiency η_p is defined as the total output power divided by the total incident power. For our example, the power transmission efficiency is $\eta_p = 0.99$ limited only by reflections (caused from the small power mismatch) and numerical issues. Moreover, illumination efficiency η_{il} can be defined as the obtained directivity divided by the theoretically maximum directivity of an aperture of the same length, that is if the output aperture fields were perfectly uniform. The measured illumination efficiency is $\eta_{il} = 0.96$ showing that the output fields have a nearly constant amplitude and phase as desired. Lastly, a total aperture efficiency $\eta_{ap} = \eta_p\eta_{il}$ is calculated, taking into account both limiting factors and measuring $\eta_{ap} = 0.95$ for the example under consideration. It should be noted that such high directivity cannot be obtained from a conventional metasurface that acts as a lens by adding a spatially-varying phase to have a planar wavefront at the output. This is because the magnitude of the output fields in such a case would be tapered according to the incident power profile. For the geometry examined, the illumination efficiency in such a case would have been only $\eta_{il} = 0.56$ due to the very small $f/D \approx 0.042$ ratio.

The output power profile of the fields in Eqs. (5)-(6) is independent of the output angle θ_{out}. Therefore, the same surface waves that have been determined through optimization for the broadside case ($\theta_{\mathrm{out}} = 0$) can be used for any other angle. Of course the HMS parameters would be different for each unit cell due to the different output fields. Various cases were examined to assess the effectiveness of the transformation with the radiation pattern of the simulations plotted in Fig. 4. As observed, the maximum radiation is effectively tilted at 20, 40 and 60 degrees off-broadside with the obtained directivity estimated at 13.7 dB, 12.7 dB and 11.1 dB, respectively. Naturally, the directivity reduces as the radiation is tilted to wider angles due to the smaller effective length of the aperture. However, in all cases it is close to the theoretically predicted one (less than 0.2 dB deviation), while the power transmission efficiency is maintained at $\eta_p > 0.91$. Lastly, the HMS parameters remain within reasonable limits for all angles, when compared with the parameters that were physically

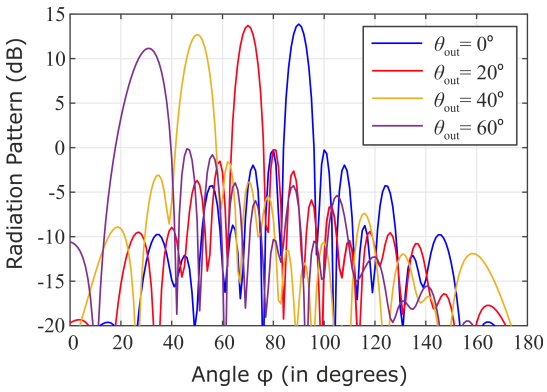

Fig. 4. Radiation pattern for different angles θ_{out} of the output aperture fields.

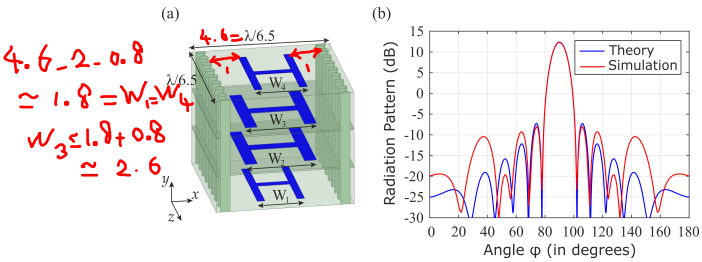

Fig. 5. Physical structure for a Taylor aperture singly-fed antenna: (a) Proposed 4-layer unit cell to implement the HMS, (b) Radiation pattern of the simulated full structure in comparison with the theoretical one.

realized for the Taylor aperture presented in the next section. This inspires confidence for the feasibility of these structures with the potential of also adding reconfigurable mechanisms to achieve dynamic scanning.

IV. Singly-fed Taylor Aperture

The proposed design framework offers a way to achieve general beamforming with a single HMS through auxiliary passively-excited surface waves. This is essential in applications where the maximum directivity is not the only specification, but compromises with the sidelobe level (SLL) are necessary. In this example a Taylor aperture antenna is designed with physical unit cells in order to demonstrate the general beamforming capabilities, but also discuss practical issues such as losses. Specifically the HMS has a length of $L_{\text{tot}} = 6\lambda$ at the operating frequency of 10 GHz and it is illuminated by an infinite magnetic linesource $\lambda/3$ away, as in the example of Sec. III. Therefore, the incident fields are given by Eqs. (3)-(4), while the output fields are determined from the analytical expressions of a Taylor (one parameter) aperture with a desired SLL of -20 dB [1].

Following the definition of input and output fields, a surface wave distribution ranging from $k_x = 1.1k$ to $k_x = 3.1k$ ($k_c = 2.1k$ and $k_w = k$ in the definition of basis-functions) is optimized to restore the local power conservation condition based on the proposed method. The details are not shown for brevity, since we focus our discussion here in the practical realization of the discretized HMS parameters. Specifically the HMS parameters Z_{se}, Y_{sm} and K_{em} are discretized in 39 sampling points leading to unit cells with lateral dimensions $\lambda/6.5 \times \lambda/6.5$. Subsequently, the theoretical response of each unit cell is represented by a network characterized by a Z matrix, as described in [4]. In order to realize the response of each unit cell, the four stacked-layer topology is utilized. While three layers are sufficient to provide any scalar omega-bianisotropic response, the addition of a fourth layer often allows to reduce the total losses. The unit cells consist of three standard Rogers RO3010 substrates of thickness $t = 1.27$ mm that are mounted together with two bondply layers RO2929 of thickness $t_b = 0.051$ mm (2 mils), as shown in Fig. 5(a). In addition, copper vias are placed between the unit cells to address intercell coupling and restore rectilinear propagation [13]. Generally, by adjusting the width of the dogbones W_i ($i \in \{1, 2, 3, 4\}$), it is possible to match the simulated network response of each unit cell to the desired one with the exception of the inevitable ohmic and dielectric losses.

After designing the unit cells individually, the whole metasurface is simulated with Ansys HFSS. The source is modeled as a small circular current loop and all copper and dielectric losses are taken into account. The far-field pattern in the forward direction is calculated and plotted in Fig. 5(b). Clearly, there is satisfactory agreement with the theoretical radiation pattern of the Taylor aperture. In particular, the obtained directivity is 12.3 dB (as compared to 12.4 dB in theory) and the SLL is -20.3 dB. Some deviations, mainly attributed to the discretization to unit cells, exist at wider angles. However, the radiated power in these angles still remains more than 20 to 25 dB lower than at broadside. Importantly, the power transmission efficiency is $\eta_p = 0.82$ including both some negligible reflections and the losses of the HMS. Although, the presence of surface waves could have increased the losses of the HMS, the addition of a fourth layer has allowed to demonstrate a simulated efficiency comparable to other HMS structures [5], [6], [13].

V. Conclusion

In conclusion, we have developed a method to design HMSs that breaks the requirement of local power conservation between the incident and the output fields. The method relies on determining the surface wave distribution that effectively redistributes the power at the input side of the HMS. Two potential applications were described, namely obtaining maximum directivity from a radiating aperture and achieving general beamforming. For the first example, it was shown through impedance-sheet simulations of the HMS that the illumination efficiency greatly outperforms the conventional metasurfaces (without excited surface waves) that act as lenses. For the second example, a Taylor pattern was realized with a physical HMS consisting of stacked-layer unit cells, showing a reasonable transmission efficiency and good agreement with the desired far-field characteristics.

ACKNOWLEDGMENT

Financial support from the Natural Sciences and Engineering Research Council of Canada is gratefully acknowledged. V. A. also acknowledges the support of the Ministry of Advanced Education and Skills Development of Ontario, the Electrical and Computer Engineering Department of the Univ. of Toronto and the Alexander S. Onassis Foundation.

REFERENCES

[1] C. A. Balanis, *Antenna Theory: Analysis and Design*, 4th ed. John Wiley and Sons, 2016.

[2] C. Pfeiffer and A. Grbic, "Metamaterial Huygens' surfaces: Tailoring wave fronts with reflectionless sheets," *Phys. Rev. Lett.*, vol. 110, p. 197401, May 2013.

[3] M. Selvanayagam and G. V. Eleftheriades, "Discontinuous electromagnetic fields using orthogonal electric and magnetic currents for wavefront manipulation," *Opt. Express*, vol. 21, no. 12, pp. 14 409–14 429, Jun. 2013.

[4] A. Epstein and G. V. Eleftheriades, "Arbitrary power-conserving field transformations with passive lossless omega-type bianisotropic metasurfaces," *IEEE Trans. Antennas Propag.*, vol. 64, no. 9, pp. 3880–3895, Sep. 2016.

[5] M. Chen, A. Epstein, and G. V. Eleftheriades, "Design and experimental verification of a passive Huygens' metasurface lens for gain enhancement of frequency-scanning slotted-waveguide antennas," *IEEE Trans. Antennas Propag.*, vol. 67, no. 7, pp. 4678–4692, July 2019.

[6] A. Epstein, J. P. S. Wong, and G. V. Eleftheriades, "Cavity-excited Huygens' metasurface antennas for near-unity aperture illumination efficiency from arbitrarily large apertures," *Nature Commun.*, vol. 7, p. 10360, Jan. 2016.

[7] B. O. Raeker and A. Grbic, "Compound metaoptics for amplitude and phase control of wave fronts," *Phys. Rev. Lett.*, vol. 122, p. 113901, Mar. 2019.

[8] A. H. Dorrah and G. V. Eleftheriades, "Bianisotropic Huygens' metasurface pairs for nonlocal power-conserving wave transformations," *IEEE Antennas Wireless Propag. Lett.*, vol. 17, no. 10, pp. 1788–1792, Oct. 2018.

[9] A. Epstein and G. V. Eleftheriades, "Synthesis of passive lossless metasurfaces using auxiliary fields for reflectionless beam splitting and perfect reflection," *Phys. Rev. Lett.*, vol. 117, p. 256103, Dec. 2016.

[10] D.-H. Kwon and S. A. Tretyakov, "Arbitrary beam control using passive lossless metasurfaces enabled by orthogonally polarized custom surface waves," *Phys. Rev. B*, vol. 97, p. 035439, Jan. 2018.

[11] D. Kwon, "Modulated reactance surfaces for leaky-wave radiation based on complete aperture field synthesis," *IEEE Trans. Antennas Propag.*, vol. 68, no. 7, pp. 5463–5477, July 2020.

[12] V. G. Ataloglou, A. H. Dorrah, and G. V. Eleftheriades, "Design of compact Huygens' metasurface pairs with multiple reflections for arbitrary wave transformations," *IEEE Trans. Antennas Propag.*, pp. 1–1, DOI: 10.1109/TAP.2020.2995423, early access on IEEE Xplore.

[13] G. Xu, S. V. Hum, and G. V. Eleftheriades, "Augmented Huygens' metasurfaces employing baffles for precise control of wave transformations," *IEEE Trans. Antennas Propag.*, vol. 67, no. 11, pp. 6935–6946, Nov. 2019.